Phased-Array Radar System Simulator (PASIM): Development and Simulation Result Assessment

Zhe Li [1,2,*], Sudantha Perera [1,2], Yan Zhang [1,2], Guifu Zhang [2,3] and Richard Doviak [4]

[1]   School of Electrical and Computer Engineering, University of Oklahoma, Norman, OK 73019, USA; sudantha@ou.edu (S.P.); rockee@ou.edu (Y.Z.)

[2]   Advanced Radar Research Center, University of Oklahoma, Norman, OK 73019, USA; guzhang1@ou.edu

[3]   School of Meteorology, University of Oklahoma, Norman, OK 73072, USA

[4]   NOAA/National Severe Storms Laboratory, Norman, OK 73072, USA; dick.doviak@noaa.gov

*   Correspondence: zhe.li-1@ou.edu; Tel.: +1-405-430-4104

check for updates

Abstract: In this paper, a system-specific phased-array radar system simulator was developed, based on a time-domain modeling and simulation method, mainly for system performance evaluation of the future Spectrum-Efficient National Surveillance Radar (SENSR). The goal of the simulation study was to establish a complete data quality prediction method based on specific radar hardware and electronics designs. The distributed weather targets were modeled using a covariance matrix-based method. The data quality analysis was conducted using Next-Generation Radar (NEXRAD) Level-II data as a basis, in which the impact of various pulse compression waveforms and channel electronic instability on weather radar data quality was evaluated. Two typical weather scenarios were employed to assess the simulator's performance, including a tornado case and a convective precipitation case. Also, modeling of some demonstration systems was evaluated, including a generic weather radar, a planar polarimetric phased-array radar, and a cylindrical polarimetric phased-array radar. Corresponding error statistics were provided to help multifunction phased-array radar (MPAR) designers perform trade-off studies.

1. Introduction

The challenge of evaluating data quality from a ground or airborne phased-array radar (PAR) system, such as multifunction phased-array radar (MPAR)/Spectrum-Efficient National Surveillance Radar (SENSR) [1], posted the need of developing an integrated system that is suitable for both simulation and measurement validations. In weather radar applications, a sub-dB accuracy of weather radar moments may be needed, such as for scattering power measurement. To accurately assess the system performance and data quality of future phased-array weather radars, the requirement for simulation fidelity is high. Various weather radar system simulators were developed before. For example, Zrnić [2] described a procedure for simulating weather-like Doppler spectra and signals, in which time series of single-polarization weather radar was generated. Galati and Pavan [3] extended Zrnić's method to dual-polarized Doppler weather radar by generating two random sequences of horizontal and vertical polarization pairs with an assigned autocorrelation coefficient and a cross-correlation coefficient. Torres [4] presented a method for simulating over-sampled dual-polarization radar signals by combining Zrnić's method and Galati's work. Cheong et al. [5] introduced a weather radar simulator which derived time-series signals from the output of a numerical weather prediction (NWP) model. Li et al. [6] presented a Monte Carlo simulation-based approach for airborne weather radars, which investigated the impacts of platform and different microphysical

parameters on the polarimetric radar variables. Byrd et al. [7] introduced a polarimetric phased-array weather radar simulator, which evaluated the impacts of cross-polar fields on weather observations and included various transmit modes. Barcaroli et al. [8] presented a validation procedure to assess the ability of a polarimetric weather radar simulator to deal with raindrop-size distributions and outputs generated by NWP models. Recently, Schvartzman et al. [9] introduced a weather radar simulator which uses existing Next-Generation Radar (NEXRAD) measurement as truth, and it was still based on a traditional frequency-domain method for polarimetric time-series generation.

Even with the achievements of prior simulations, data quality prediction and analysis for MPAR remain a challenge due to limitations. Firstly, using NWP model outputs as weather truth fields is limited to specific scenarios and events that are not sufficient for a comprehensive and realistic representation for all different operational cases. It is more reasonable to use real measurement fields. Secondly, although antenna patterns are widely included in studies such as Reference [7], the impacts of phased-array radar electronics are as important to data quality in practical applications, and transient response of the radar electronics, thus, needs to be considered. Distortions caused by amplifier nonlinearity, phase shifter quantization, or any instabilities of the array elements were reported to affect the overall system performance and data quality [10,11]. Weather measurements are highly sensitive to such effects. However, none of the current weather radar system simulators take them into account. Thirdly, pulse compression waveforms are increasingly used in weather radars, especially in PARs. To better estimate the data quality based on different PAR waveforms and predict the spectrum compliance of the transmitters, we should be able to precisely simulate the time-domain data sequences. Current simulations ignore the transient behaviors of electronics and weather scatterers. In future multi-function systems, however, longer pulses with wider bandwidth tend to be used. Lastly, for multi-mission PAR, the time-scheduling of radar resources (such as power-aperture dwell time) for adaptive scanning or target tracking functions requires the simulation execution in time steps for better system-level evaluations.

The proposed solution, which is called phased-array radar system simulator (PASIM), is a newly developed, time-domain simulation software package that utilizes the operational NEXRAD Level II data as the basis of weather truth fields. Usage of such data is more of an engineering solution rather than of meteorological significance. A covariance matrix-based method is applied for time series simulation. The simulation process employs time-domain system updates and electronic behavior models to address the combined effects of antennas, transmit/receive (T/R) modules, and pulse compression waveforms. By using the functions in the MATLAB Phased-Array System Toolbox and other tools, the software is intrinsically based on time-step simulations. The new simulation approach can address the challenges of large-scale system data quality prediction and adds new insights into the system design validations.

Based on the improved simulation methods and tools, a more systematic approach for data quality assessments for future PAR weather surveillance systems is developed. Performance evaluation metrics, including bias and standard deviation of the estimated polarimetric weather radar moments compared to the truth fields, are direct outputs from the simulation system. Furthermore, example radar system configurations are evaluated, including the configurations of array manifolds, waveforms, and processing schemes. As such, we can evaluate how the data quality differs and what design approaches are recommended for the best trade-off under different types of weather.

This paper is organized as follows: Section 2 details the PAR system simulation methods and techniques used by PASIM. Section 3 provides system design examples and data quality analysis based on the system-specific architectures and different weather scenarios. Section 4 presents the summary and conclusions.

2. PASIM System Design

2.1. Simulation Framework

In PASIM, all basic radar subsystems are modeled as system objects, including a waveform generator, transmitter, antenna, platform, weather target, propagation path, receiver, etc. The parameters can be defined flexibly to support system-level trade-off analysis. When a radar scans an area of interest, at each scan angle, radar and target positions can be updated based on their motions. Then, the target (radar resolution cell) angles seen by the radar beams are calculated. After that, a steering vector of the current scan angle is computed, from which a radar beam is formed. During each dwell time, a pulse containing the designed transmit waveform is generated, amplified by the transmitter object and then radiated by the antenna ("radiator") object. When the radiated electromagnetic (EM) waves interact with the weather targets, they are reflected and collected by the antenna ("collector") objects. Then, the return signals are amplified by the receiver and beamformed, passed through a matched filter, and stored into a three-dimensional (azimuth × range × pulse) data cube. During this process, if the receiver sampling rate is sufficiently high, the transmitted and received signals can be computed based on time-step evolution from a pulse to the next.

Currently, NEXRAD Level II data are used as input into the simulator and sampled as "truth fields". Note that the NEXRAD data here are not meteorological truth fields, but measured radar moments from NEXRAD. Based on phased-array radar system specifications, modeling parameters, and antenna pattern measurements, an end-to-end system simulation can be conducted, and the in-phase and quadrature time series (I & Q) data can be obtained and saved as a data cube. Subsequently, the data cube is fed into a signal-processing chain to obtain polarimetric moment estimates. Finally, these estimates are compared with NEXRAD Level II data, and error statistics are obtained.

In Figure 1, the structure of PASIM with its functional blocks, and how these blocks are implemented using different programming languages are depicted. The radar system simulation and the testing scenario are based on NEXRAD Level II data. Additional meteorological data are also obtained through the Advanced Weather Interactive Processing System (AWIPS), which can be used to improve the ground-truth data of the weather scenarios and provide a data quality visualization. The system component (antenna, T/R module, and digital backend) parameters are obtained from available commercial products. The core of the implementation is based on the MATLAB Phased-Array System Toolbox [12,13] and other toolboxes. Customized models include signal-processing modules and electronics models. The output of the simulator is a data quality analysis report.

Specifically, in Figure 1, the input blocks comprise three parts. The "NEXRAD Moment Data" refer to NEXRAD Level II data available from the National Climatic Data Center, and the data are read by the Python ARM Radar Toolkit (Py-ART), which is an open-source software package widely used in the weather radar community [14,15]. The "Vendor/System Component Test Data/Transient Response Data" refer to the radar component parameters used in a real phased-array radar system, such as the datasheet of an AD9361/9371 radio frequency (RF) transceiver, the nonlinear response curve of a high-power amplifier (HPA), etc. The "Radar Parameters" contain user-specific radar system specifications, including waveform (simple rectangular, pulse compression, etc.), array manifolds (planar, cylindrical, etc.), scanning strategy (plan position indicator (PPI), range height indicator (RHI), volume scan, etc.), and so on. The "Time-Domain System Simulation" block is the core of PASIM, which employs the MATLAB Phased-Array System Toolbox, RF/Communications Toolbox and electronics models to perform end-to-end time-domain radar system simulations, as shown in Figure 2a, whose output is time-series data organized in a three-dimensional data cube. The "Weather Radar Data Quality Prediction" block produces the radar data quality analysis report. Figure 2b summarizes the overall data flow of weather radar data quality prediction. Time series for all the radar transceiver channels are organized into a data cube, which is fed into the weather radar signal-processing chain to compute spectral moments and polarimetric moments. The moment estimation outputs are compared

with the NEXRAD Level-II data to produce a data quality report in the form of statistical errors such as bias and standard deviation.
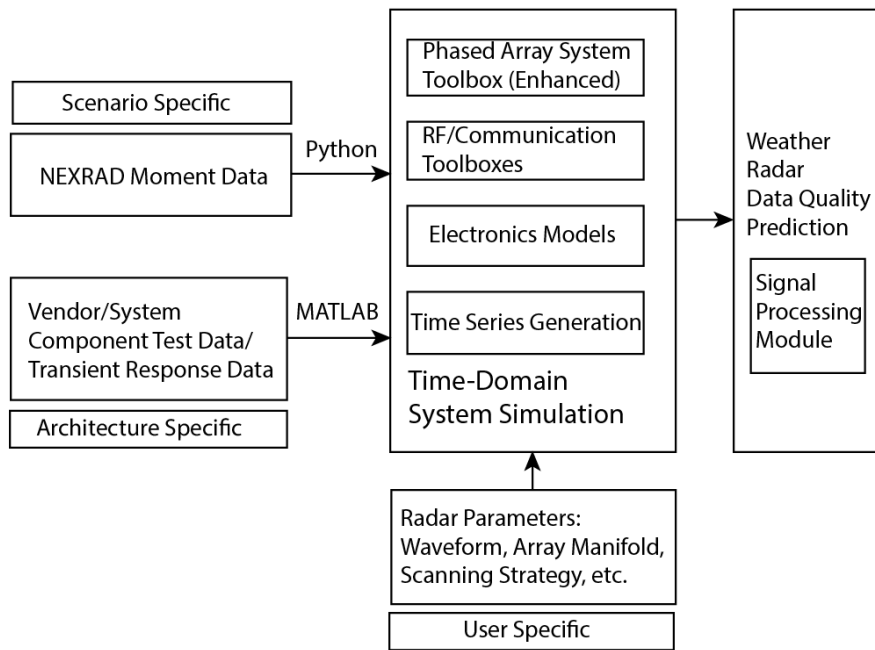

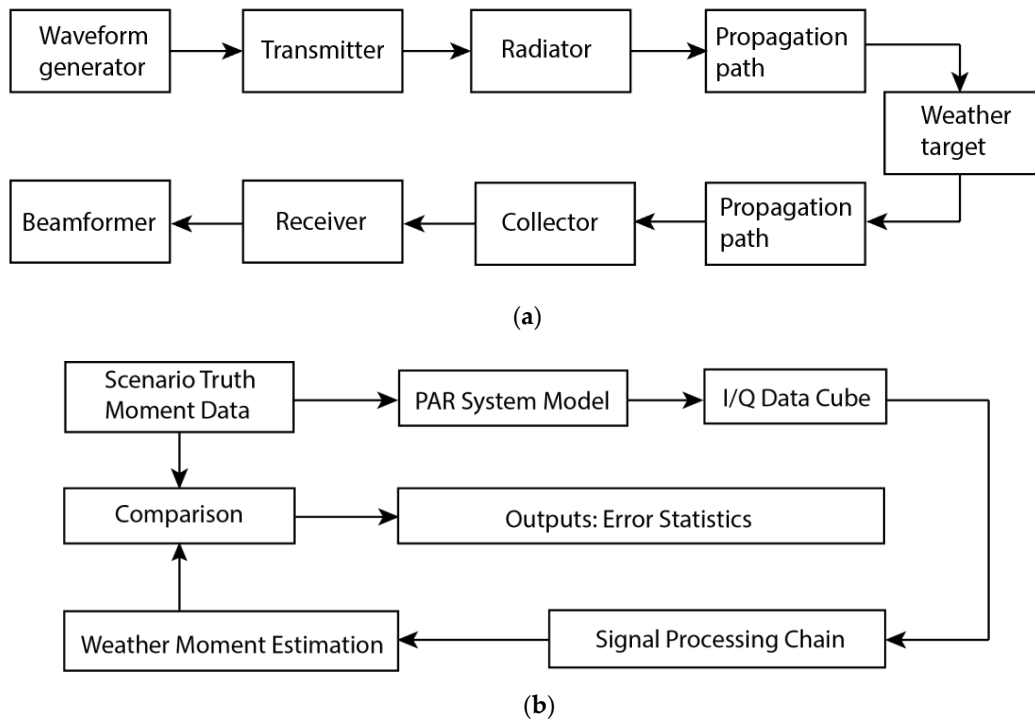**Figure 1.** The structure of phased-array radar system simulator (PASIM).

Figure 2. Operations of the key modules of PASIM: (**a**) time-domain system simulation; (**b**) weather radar data quality prediction.

2.2. Subsystems

In this section, key subsystems in PASIM that have major impacts on weather data quality are introduced, which include antennas, T/R modules, and RF transceivers, as well as waveforms.

2.2.1. Antennas

In PASIM, the phased-array radar is placed on a platform, whose position, velocity, and acceleration can be defined. The orientation axes of the platform can be manipulated by a rotation matrix, making it suitable for both ground-based and airborne applications. Furthermore, effects of electronic scanning such as beam broadening and scan loss are incorporated. Both the element radiation pattern and array pattern can be imported from EM simulations or chamber measurements. Moreover, the antenna element is modeled to have polarization diversity by specifying polarized radiation patterns. For instance, realistic dual-polarized patch and crossed-dipole elements are included, whose horizontal and vertical polarization components can be transmitted simultaneously or alternately to measure the target scattering matrix. The array axis can be specified flexibly so that array elements are located along the selected coordinate system axis. The computation of the array factor supports a linear array, planar array, circular array, and conformal array, while beam steering and beamforming are implemented by applying complex weights to the individual elements of the array. To accelerate the computations, a full array can be partitioned into one or more subarrays, and each subarray can be steered independently. As an example, Figure 3a,b show a dual-polarized patch element and its three-dimensional (3D) radiation pattern, Figure 3c shows an 8 × 8 planar subarray using this antenna element, while Figure 3d,e show the azimuth cut and elevation cut for the synthesized array pattern of an 80 × 80 planar array using PASIM, which is formed from 100 of the 8 × 8 subarrays. The basic parameters of the antenna element and array are listed in Table 1.
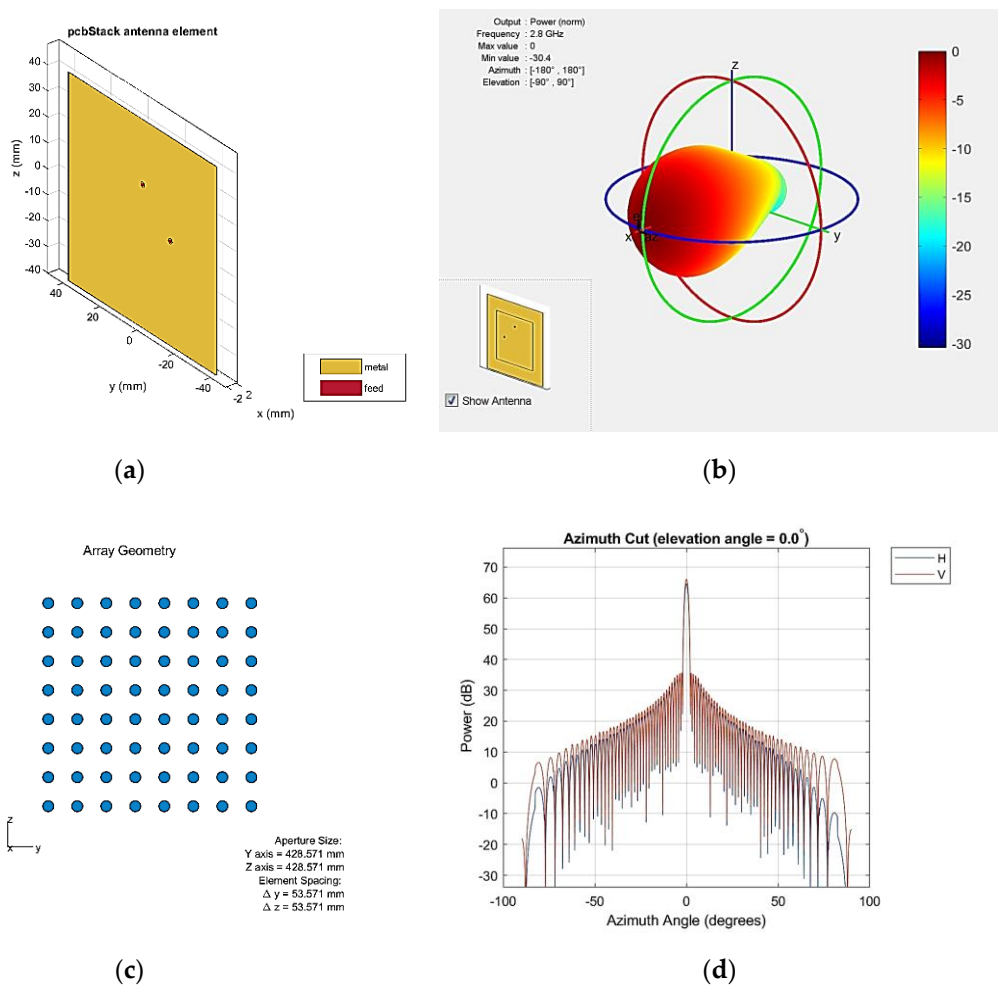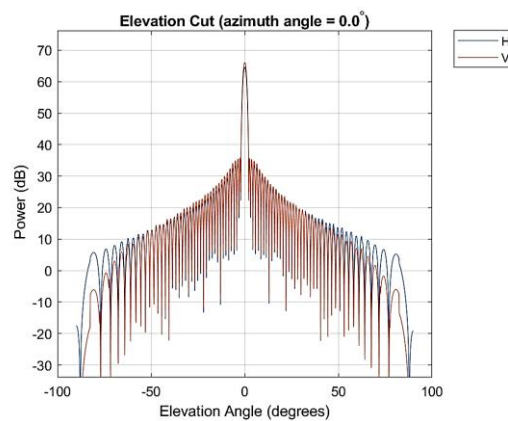

(a)

(b)

(c)

(d)

Figure 3. *Cont.*

(**e**)

Figure 3. The antenna radiating element and array constructed in PASIM: (**a**) a simple patched element; (**b**) three-dimensional (3D) radiation pattern of the patch element; (**c**) an 8×8 planar subarray; (**d**) azimuth cut for the synthesized radiation pattern of an 80×80 planar array; (**e**) elevation cut for the synthesized radiation pattern of an 80×80 planar array.

Table 1. The basic parameters of the antenna element and array.

Parameter	Value
Type	Patch
Size	5.24×5.24 cm
Polarization	Dual linear polarized
Transmit	Yes
Receive	Yes
Number of elements in azimuth	80
Number of elements in elevation	80

2.2.2. T/R Modules and RF Transceivers

For a multi-channel polarimetric radar system, electronic instability from pulse-to-pulse (P2P) and channel-to-channel (C2C) needs to be modeled, including high-power amplifier (HPA) distortions and instabilities in RF transceiver channels, quantization error of phase shifters and attenuators in T/R modules, imbalance of the power combiners and splitters in each channel, fluctuation in receiver noise floor, phase variations caused by local oscillator and reference clock instability, and so on. Among all these factors, HPA complex gain (including amplitude and phase) variation due to thermal effects, which may reduce the system coherency [16], is a major source of electronic instability. Accordingly, several mathematical models were developed to characterize the nonlinear behavior of HPA, such as the Saleh model, Volterra series model, complex power series model, and Hammerstein–Wiener model [10]. In this study, the Saleh model is used as a simple two-parameter function to depict the amplitude-to-amplitude (AM-to-AM) and amplitude-to-phase (AM-to-PM) characteristics of nonlinear amplifiers. Ideally, the input signal to the amplifier is expressed as [17]

$$x(t) = r(t) \cos[\omega_0 t + \varphi(t)], \tag{1}$$

where ω_0 is carrier frequency, and $r(t)$ and $\varphi(t)$ are the amplitude and phase of the modulated signal, respectively. The distorted output of the nonlinear amplifier is

$$y(t) = A[r(t)] \cos[\omega_0 t + \varphi(t) + \Phi[r(t)]], \tag{2}$$

where $A[r(t)]$ refers to AM-to-AM conversion, and $\Phi[r(t)]$ refers to AM-to-PM conversion. Specifically, these two functions can be expressed as

$$A(r) = \frac{\alpha_a r}{1 + \beta_a r^2}, \tag{3}$$

$$\Phi(r) = \frac{\alpha_\phi r^2}{1 + \beta_\phi r^2}. \tag{4}$$

As an example, the optimum parameters for a solid-state power amplifier were selected as $\alpha_a = 2.1587$, $\beta_a = 1.1517$, $\alpha_\phi = 4.0033$, and $\beta_\phi = 9.1040$. Figure 4a shows the ideal and distorted envelope of a 60-dB Taylor-windowed linear frequency modulation (LFM) waveform, and Figure 4b compares autocorrelation function (ACF). As can be seen, after the Saleh nonlinearity model is incorporated into the amplifier, the Taylor-windowed LFM waveform is distorted, and the matched filter output shows increased range sidelobes which are undesirable.
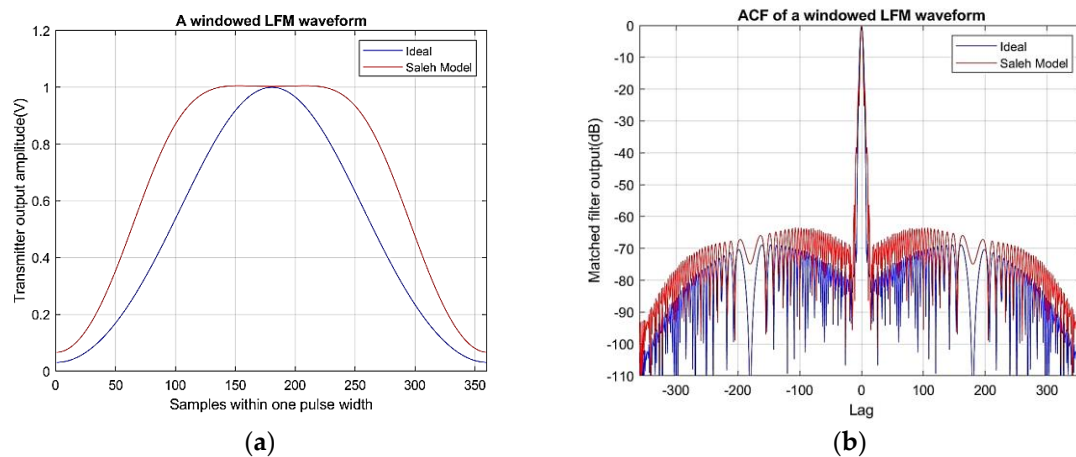

(a) **(b)**

Figure 4. The impact of the Saleh nonlinearity model on an example of a 60-dB Taylor windowed linear frequency modulation (LFM) waveform and autocorrelation function (ACF): (**a**) distortion of the waveform envelope; (**b**) ACF of the waveform before and after nonlinear distortion.

On the other hand, the C2C spatial instability in a PAR can be evaluated in PASIM as well. The C2C amplitude instability mainly distorts antenna pattern, while C2C phase instability will both distort antenna pattern and increase phase noise. Another C2C error comes from T/R module failure, which distorts antenna pattern by raising sidelobes and reducing gain. Also, the impact of quantization error introduced by the phase shifter and the resultant data quality can also be assessed using PASIM. These errors are included during the beamforming process. As an example, a circular array with a diameter of 10 m is simulated. A 90° sector consisting of 156 patch elements is excited to form a beam of 1.1° beamwidth. Then, a Taylor tapering is applied to keep the pattern sidelobes below −30 dB, which matches the NEXRAD requirements as shown in Section 3.1. The C2C random amplitude and phase errors are modeled as Gaussian distribution variables with zero mean and standard deviation of 0.5 dB and 6°, respectively, and the system has a 5% probability of element failures. It is assumed that 5-bit phase shifters are used. Figure 5a shows the array patterns as impacts from the random amplitude and phase errors, whereas Figure 5b shows the array patterns without quantization error and with quantization errors based on 5-bit phase shifters.
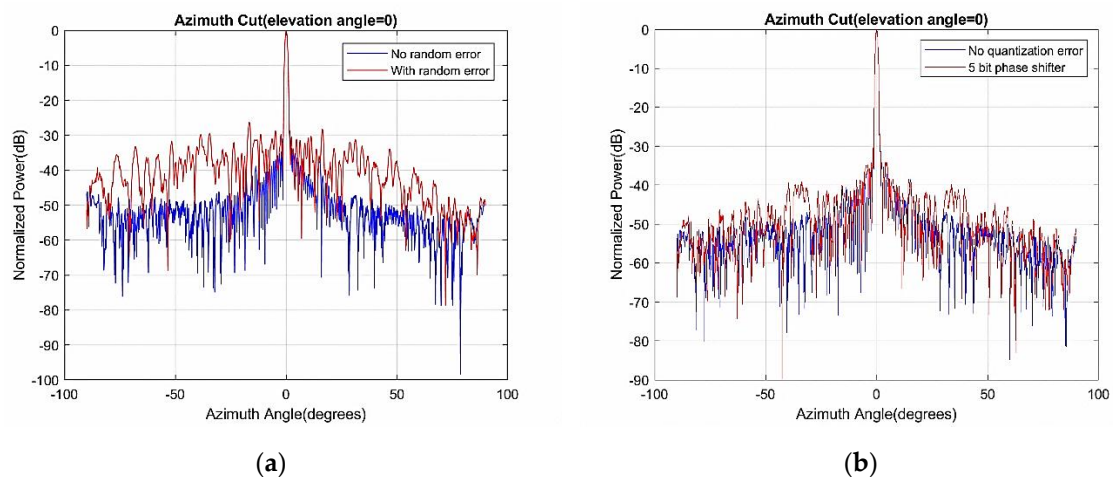
Figure 5. Typical array radiation patterns in PASIM by incorporating the impact of channel-to-channel (C2C) instability: (**a**) impacts of the random channel amplitude and phase errors; (**b**) impacts of phase shifter quantization error based on 5-bit phase shifters.

2.3. Waveforms

In PASIM, various pulse compression waveforms can be selected, and their impacts on weather radar data quality can be evaluated. As an example, an LFM waveform, a Taylor-windowed LFM waveform, and an optimized nonlinear frequency modulation (NLFM) waveform are implemented and compared. The "generic radar" parameters for this simulation are shown in Section 3.3.1. The bandwidth of the NLFM waveform is 3.6 MHz, and the transmit pulse width is 50 μs. This example NLFM waveform uses Gaussian function as a spectral density function, which can achieve a sidelobe level below -70 dB without amplitude weighting (thus, no loss of signal-to-noise ratio (SNR)) [18]. The windowed LFM uses a Taylor window with a maximum sidelobe level of -60 dB below the mainlobe peak so that it can achieve a similar level of range sidelobe as of the NLFM waveform. Figure 6 plots the matched filter outputs, reflectivity estimation outputs, and scatter plot of the reflectivity estimation (truth vs. estimation) for the three waveforms, from a simulated sector scan of a tornado case. It can be found that the high range sidelobes (around -13 dB) of the LFM waveform exert an obvious impact on reflectivity data quality. For instance, Figure 6b shows that stronger echoes in nearer range contaminate the relatively weak echoes in the northwest corner. This is also validated by Figure 6c which shows a larger deviation in low-reflectivity regions. Also, error statistics indicate that the standard deviation of estimated reflectivity compared to NEXRAD reflectivity for the LFM waveform reaches 1.19 dB, which does not meet the NEXRAD requirements as shown in Section 3.1. For the windowed LFM waveform, while it can achieve lower range sidelobe levels, its power efficiency is only 0.35 as a result of aggressive windowing. Due to reduced transmit power, the estimates in low-reflectivity regions have larger errors, as shown in Figure 6f. Moreover, the standard deviation of the estimated reflectivity is 1.14 dB, which still does not meet the NEXRAD requirements, as shown in Section 3.1. As a comparison, for the NLFM waveform whose power efficiency is 0.87, most of the relatively weak echoes in the northwest corner can be observed in Figure 6h, and the scatter plot in Figure 6i indicates that the reflectivity estimates are consistent with the NEXRAD truth. For this case, the error statistics show that the standard deviation of estimated reflectivity is 0.80 dB, which meets the NEXRAD data quality requirement.
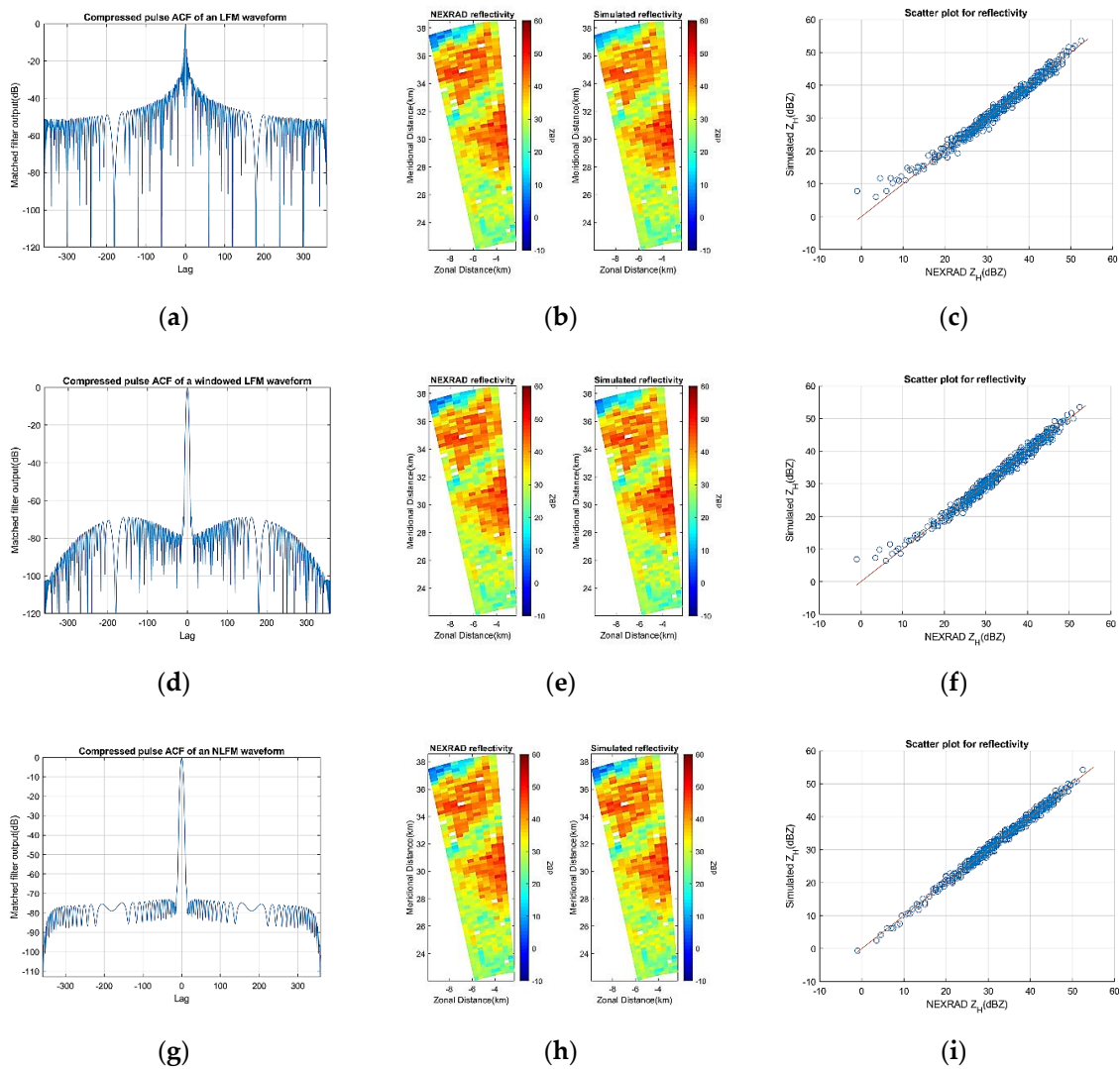
Figure 6. Examples of PASIM scan outputs, when the specific waveforms of an LFM, a Taylor-windowed LFM, and an example nonlinear frequency modulation (NLFM) waveform are used to estimate reflectivity (Z_H) of a sector scan for a tornado case: (**a**) matched filter output for LFM; (**b**) simulated Z_H for LFM; (**c**) Z_H scatter plot for LFM; (**d**) matched filter output for windowed LFM; (**e**) simulated Z_H for windowed LFM; (**f**) Z_H scatter plot for windowed LFM; (**g**) matched filter output for NLFM; (**h**) simulated Z_H for NLFM; (**i**) Z_H scatter plot for NLFM.

2.4. Time-Series Generation and Signal Processing

2.4.1. Monte Carlo Method

In PASIM, there are two possible ways to model the randomness of weather scatterers in space and time. The first one is Monte Carlo method. That is, in each resolution volume, the total backscattered wave field is calculated by summation of the contributions from each scatterer. To simplify the model, it is assumed that all the scatterers in the resolution volume have the same size. According to the definition of reflectivity [19–21],

$$Z_{hh} = \frac{4\lambda^4}{\pi^4 |K_w|^2} \int |s_{hh}|^2 N(D)dD = K \int |s_{hh}|^2 N(D)dD. \tag{5}$$

The horizontal scattering amplitude of each scatterer can be obtained as

$$|s_{hh}| = \sqrt{Z_{hh}/K/N}, \tag{6}$$

where Z_{hh} is the horizontal reflectivity in the linear scale, λ is the wavelength of an electromagnetic wave, D is the drop diameter, $N(D)$ is the drop size distribution, K_w is the dielectric constant factor of water, and N is the number of scatterers in the resolution volume. Accordingly, the vertical scattering amplitude of each scatterer can be calculated as

$$|s_{vv}| = \frac{s_{hh}}{\sqrt{Z_{dr}}}, \tag{7}$$

where Z_{dr} is the differential reflectivity in the linear scale.

At each pulse repetition time (PRT), the scatterers' position and velocity update according to the Doppler velocity and spectrum width. It is assumed that the copolar correlation coefficient ρ_{hv} is reduced by a factor of $e^{-\sigma_\delta^2/2}$ due to the random scattering phase difference, where σ_δ is the standard deviation of scattering phase difference [19]. That is, $\rho_{hv} = e^{-\sigma_\delta^2/2}$. As a result,

$$\sigma_\delta = \sqrt{-2\ln(\rho_{hv})} = \sqrt{\sigma_{\delta h}^2 + \sigma_{\delta v}^2}. \tag{8}$$

For simplicity, PASIM uses $\sigma_{\delta h} = \sigma_{\delta v} = \sigma_\delta/\sqrt{2}$, where $\sigma_{\delta h}$ and $\sigma_{\delta v}$ are standard deviations of horizontal backscattering phase φ_h and vertical backscattering phase φ_v, respectively. The complex scattering amplitudes for a scatterer are expressed as

$$s_{hh} = |s_{hh}| \cdot e^{j\varphi_h}, \tag{9}$$

$$s_{vv} = |s_{vv}| \cdot e^{j\varphi_v} \cdot e^{j\phi_{DP}}, \tag{10}$$

where ϕ_{DP} is the differential phase. The total complex backscattering amplitudes of the resolution volume are

$$S_{hh} = \sum_{l=1}^{N} s_{hh_l} \cdot e^{-jk_d \cdot r} = \sum_{l=1}^{N} s_{hh_l} \cdot e^{-j2k_i \cdot r_l}, \tag{11}$$

$$S_{vv} = \sum_{l=1}^{N} s_{vv_l} \cdot e^{-jk_d \cdot r} = \sum_{l=1}^{N} s_{vv_l} \cdot e^{-j2k_i \cdot r_l}, \tag{12}$$

where N is the total number of scatterers in the volume, and k_i and k_d are incident and backscattering wave vectors, respectively. Each resolution volume is equivalent to a "single scattering center". The scattering center is an equivalent point target that produces the same scattering amplitudes as the volume does. S_{hh} and S_{vv} are related to the scattering matrix element of the equivalent scattering center by a scaling factor, and S_{hh} and S_{vv} are updated at each time step (PRT) according to the updated distribution of the hydrometeors' position and velocity within the resolution volume.

2.4.2. Covariance Matrix Method

Generating I/Q time-series data based on the statistical correlation among pulses and polarizations is the second method in PASIM. Firstly, two independent random signals V_1 and V_2 are generated, which follow Gaussian distribution with zero-mean and their standard deviations are derived from reflectivity values. According to Reference [20], the autocorrelation function of the received signals is given by

$$R(mT_s) = S \cdot e^{-8\left(\frac{\pi\sigma_v mT_s}{\lambda}\right)^2} \cdot e^{-j\frac{4\pi\bar{v}mT_s}{\lambda}} + N \cdot \delta_m, \tag{13}$$

where S is the average signal power, $\overline{v}$ and σ_v refer to the mean radial velocity and spectrum width of the radar resolution volume filled by precipitation, m is the index ("lag") of the pulse ($0 \leq m \leq M - 1$, where M is the number of pulses in the dwell time), T_s is the pulse repetition time, N is the mean white noise power, and δ_m is 1 for $m = 0$ and zero otherwise. Based on Equation (13), a complex covariance matrix C, which is an M-by-M Hermitian positive-definite matrix, can be constructed. Using Cholesky decomposition, C may be decomposed as

$$C = P \cdot P^*, \tag{14}$$

where P is an M-by-M upper triangular matrix from the diagonal and upper triangle of covariance matrix C. Then, P is applied to V_1 and V_2 as

$$V_1 = V_1 \cdot P, \tag{15}$$

$$V_2 = V_2 \cdot P. \tag{16}$$

Next, the complex scattering amplitudes of the resolution volume are generated as

$$S_{hh} = V_1, \tag{17}$$

$$S_{vv} = \left[\rho_{hv} \cdot V_1 + \sqrt{1 - \rho_{hv}^2} \cdot V_2 \right] \cdot \frac{e^{j\phi_{DP}}}{\sqrt{Z_{dr}}}. \tag{18}$$

As a comparison, both the Monte Carlo method and covariance matrix method are statistical methods. Generally, the Monte Carlo method is more representative of the physical process in the real world, as it assumes that there are multiple scatterers within each resolution volume, but it will take more time to run the simulation, while the covariance matrix method is more computationally efficient. A large number of simulations show that both methods can achieve similar moment estimation accuracy when other radar system parameters are the same.

The main radar components, parameters, and models used in the simulations are listed in Table 2.

Table 2. Summary of the main radar components, parameters, and models used in the simulations. HPA—high-power amplifier.

Radar Component/Parameter/Model	Value
Antenna element	Dual-polarized patch
HPA nonlinearity	Saleh model
Digital phase shifter	5-bit
Waveform	Rectangular pulse
Weather target model	Covariance matrix

3. System-Specific Examples and Data Quality Predictions

3.1. Requirements

PASIM is used as a system trade-off study tool such as for the data quality prediction of MPAR/SENSR radar and spectrum compliance investigations. The requirement of data quality analysis is providing high-level guidance for engineering designers to perform trade-off analysis and risk mitigations in the early stage of system design. For example, analysis can provide a range of error margins of weather radar products for a given waveform design that complies with the National Telecommunications and Information Administration (NTIA) spectrum masking. In this section, solutions and techniques described in Section 2 are applied to specific radar systems. Bias and standard deviation of the main weather radar products are used as the performance metrics [22], as listed in Table 3. As this paper mainly focuses on polarimetric moment evaluation, data quality of Doppler moments such as radial velocity and spectrum width are not listed in later sections. To

evaluate Doppler moments, a different scanning strategy (such as shorter pulse repetition time) needs to be employed to mitigate velocity aliasing, which is different from the configuration of polarimetric moment measurements.

Table 3. Next-Generation Radar (NEXRAD) requirements of data quality for basic weather radar moments.

Radar Variable	Bias	Standard Deviation
Reflectivity	1 dB	1 dB
Radial velocity	1 m/s	1 m/s
Spectrum width	1 m/s	1 m/s
Differential reflectivity	0.1 dB	0.2 dB
Correlation coefficient	0.005	0.01
Differential phase	1°	2°

3.2. Configuration of System Examples and Weather Scenarios

In addition to a generic radar reference with a similar configuration to NEXRAD, two PAR systems with different array manifolds were used as examples for data quality evaluations. The first system example was the Advanced Technology Demonstrator (ATD) [23,24], which is a planar array being tested by the National Severe Storms Laboratory (NSSL) of the National Oceanic and Atmospheric Administration (NOAA). The other example was the Cylindrical Polarimetric Phased-Array Radar (CPPAR) [25,26], which uses a cylindrical polarimetric array with commutated beams, such that the antenna patterns are invariant with respect to azimuth scan angles. The azimuth-invariant beams can enhance polarimetric pattern isolations. Because the focus of the examples was demonstrating the impact of antenna pattern synthesis, we assumed these systems used the same waveform (1.6 µs rectangular pulse), and the channel electronics used generic parameters as the Saleh model for the amplifier and a 5-bit phase shifter in Section 2.2.2.

Two representative weather scenarios were considered. The first scenario was an intense tornado with a large reflectivity gradient in the field of view. The tornado event occurred in Moore, Oklahoma at 8:08 p.m. coordinated universal time (UTC) on 20 May 2013, in which Level-II data from KTLX radar (an operational NEXRAD) were used as weather truth fields. The second case was convective precipitation with a relatively uniform weather field distribution, which was also observed by KTLX radar on 4:33 a.m. UTC on 19 May 2013. In each case, a sector of a PPI scan with 0.5° elevation, which mainly consists of precipitation area, was selected for PAR simulations. Since the two events were observed by the same NEXRAD within two consecutive days, the time-variant NEXRAD system drift was small, which is beneficial for consistent data quality evaluations.

3.3. Data Quality Results from PASIM

3.3.1. Generic Radar

A generic SENSR radar system was simulated, whose parameters were chosen to match the key system parameters of NEXRAD as listed in Table 4.

After PASIM generated the I/Q data cubes, the pulse pair processing (PPP) method was employed to estimate the polarimetric weather radar moments. Both the tornado and the convective precipitation cases were used as weather truth fields. In the tornado case, a northern sector of the PPI image that mainly consisted of precipitation is plotted in Figure 7, which shows that all the simulated polarimetric moments were consistent with the truth fields, and error statistics are provided in Section 3.3.4. The major source of estimation error was found to be the sidelobes of the antenna pattern, which was validated by the fact that, if the sidelobe level was negligible, the standard deviation for estimated Z_H and Z_{DR} both reduced to 0.01 dB.

Table 4. System specifications of a generic radar.

Radar Parameters	Values
Frequency	2800 MHz
Antenna Gain	45.5 dB
Beamwidth	1.0°
First sidelobe	−32 dB
Waveform	Rectangular pulse
Pulse width	1.6 μs
Pulse repetition frequency	300 Hz
Range resolution	250 m
Peak power	700 kW
Noise figure	2.7 dB
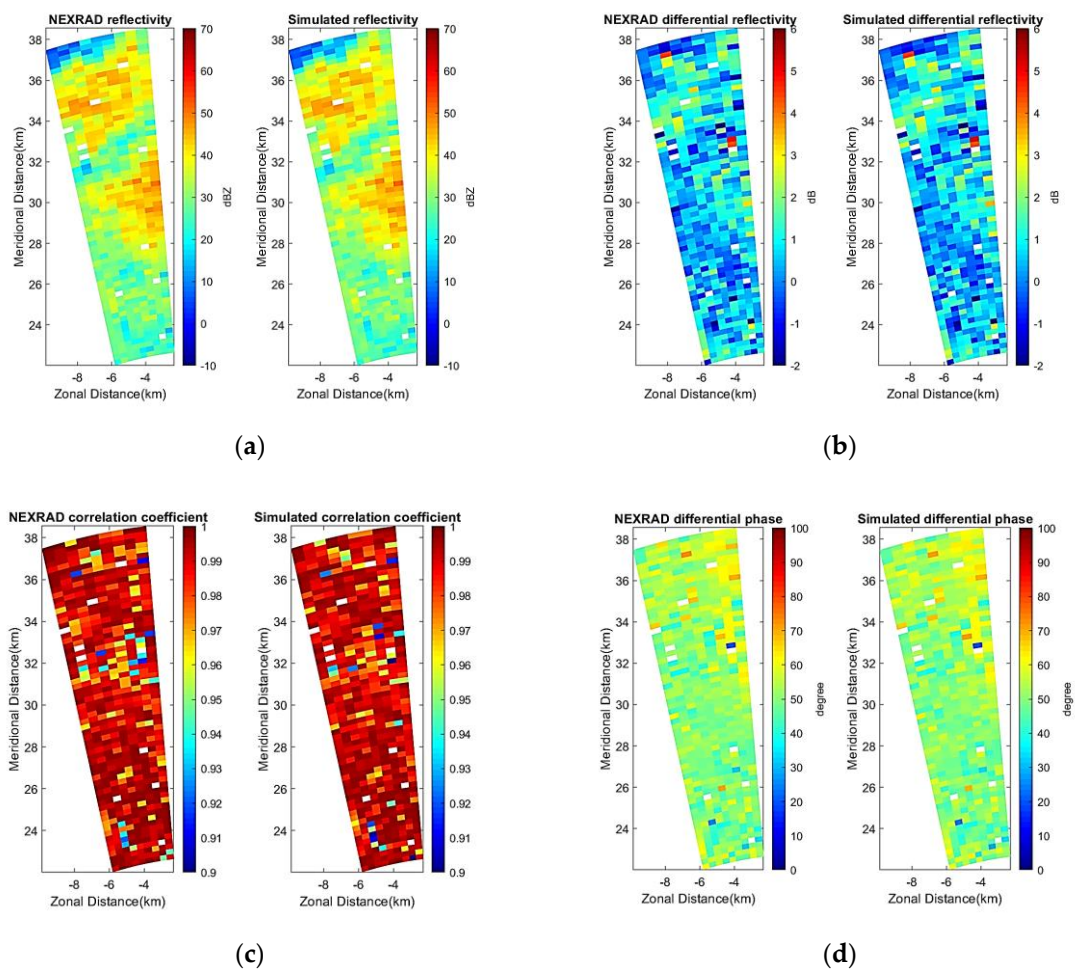
Figure 7. Simulated weather radar moments from the generic radar example, and comparison with the Nest-Generation radar (NEXRAD) "truth" fields for Case 1: (**a**) reflectivity, (**b**) differential reflectivity, (**c**) correlation coefficient, (**d**) differential phase.

For the convective precipitation case, a larger sector spanning 90° in azimuth comprising more uniform weather fields was selected. As can be seen in Figure 8, the simulated moments were also consistent with NEXRAD truth fields. Error statistics are provided in Section 3.3.4, which can also meet the requirements in Table 3.
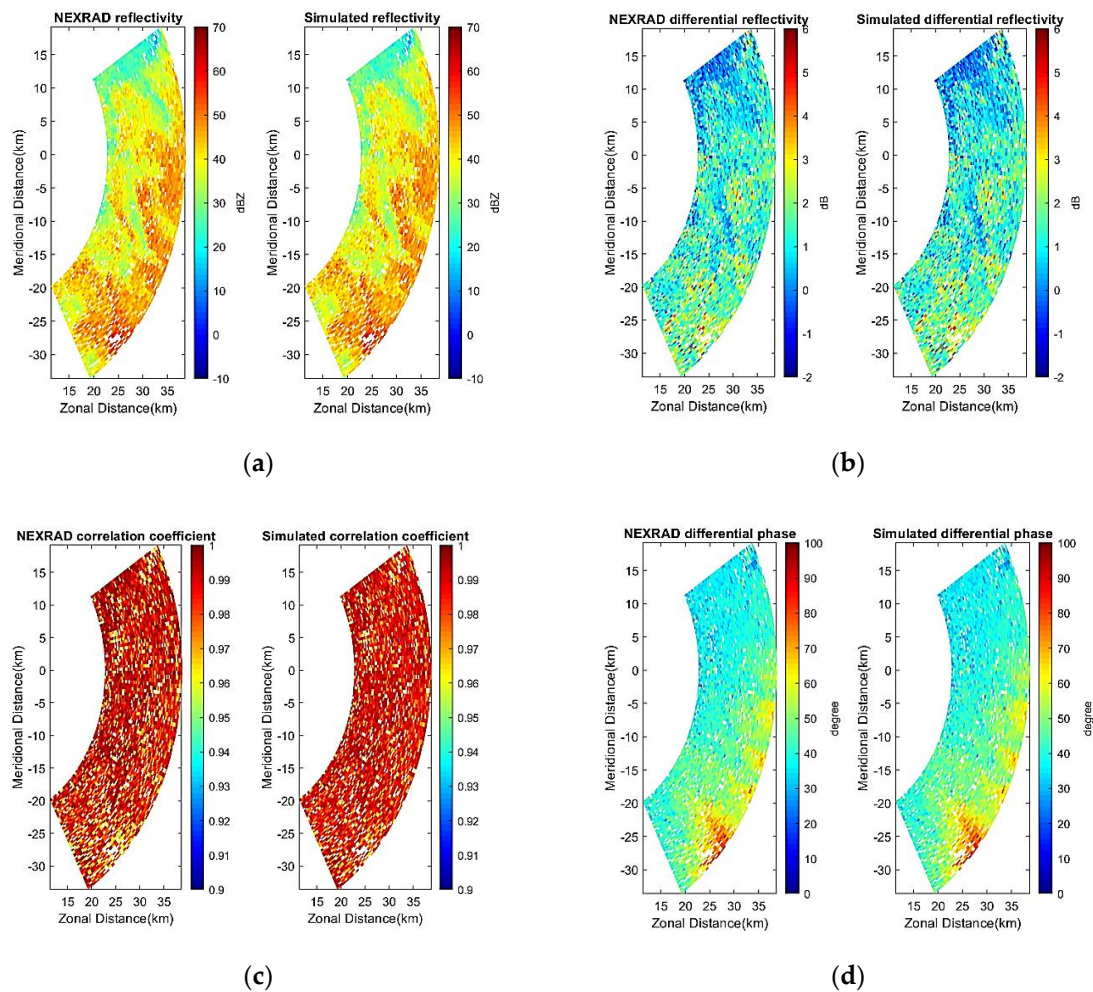
Figure 8. Simulated weather radar moments from the generic radar example, and comparison with the NEXRAD "truth" fields for Case 2: (**a**) reflectivity, (**b**) differential reflectivity, (**c**) correlation coefficient, (**d**) differential phase.

3.3.2. Advanced Technology Demonstrator (ATD)

To implement a testbed of a larger scale planar polarimetric phased-array radar (PPPAR) for weather and air-traffic observation, ATD, which is an S-band dual-polarization active phased-array radar with 4-m aperture size, was initially deployed in Norman, Oklahoma in 2018 [24]. The technical specifications of ATD, which are relevant to PASIM, are listed in Table 5. Again, both the tornado and the convective precipitation cases were simulated, while, for the PPPAR system, the "uniform" weather fields in the second case provided more insights into the weather radar data quality. Note that PASIM used a simplified dual-polarized patch antenna model as described in Section 2.2.1. The PASIM outputs of the polarimetric moments and the average Z_{DR} bias along the azimuth dimension are shown in Figure 9. Error statistics for Case 1 and Case 2 are provided in Section 3.3.4, respectively.

As can be seen, simulated moments appeared to be a little bit "smeared" compared to the truth fields due to the broader beamwidth of ATD than NEXRAD. More importantly, as the array beam scanned away from the broadside, the Z_{DR} bias increased, which is consistent with the two-way power ratio of horizontal and vertical patterns that is dependent on azimuth. The system Z_{DR} bias values match the theoretical results in References [27,28], which further confirms that ATD requires Z_{DR} calibration at each azimuth radial.
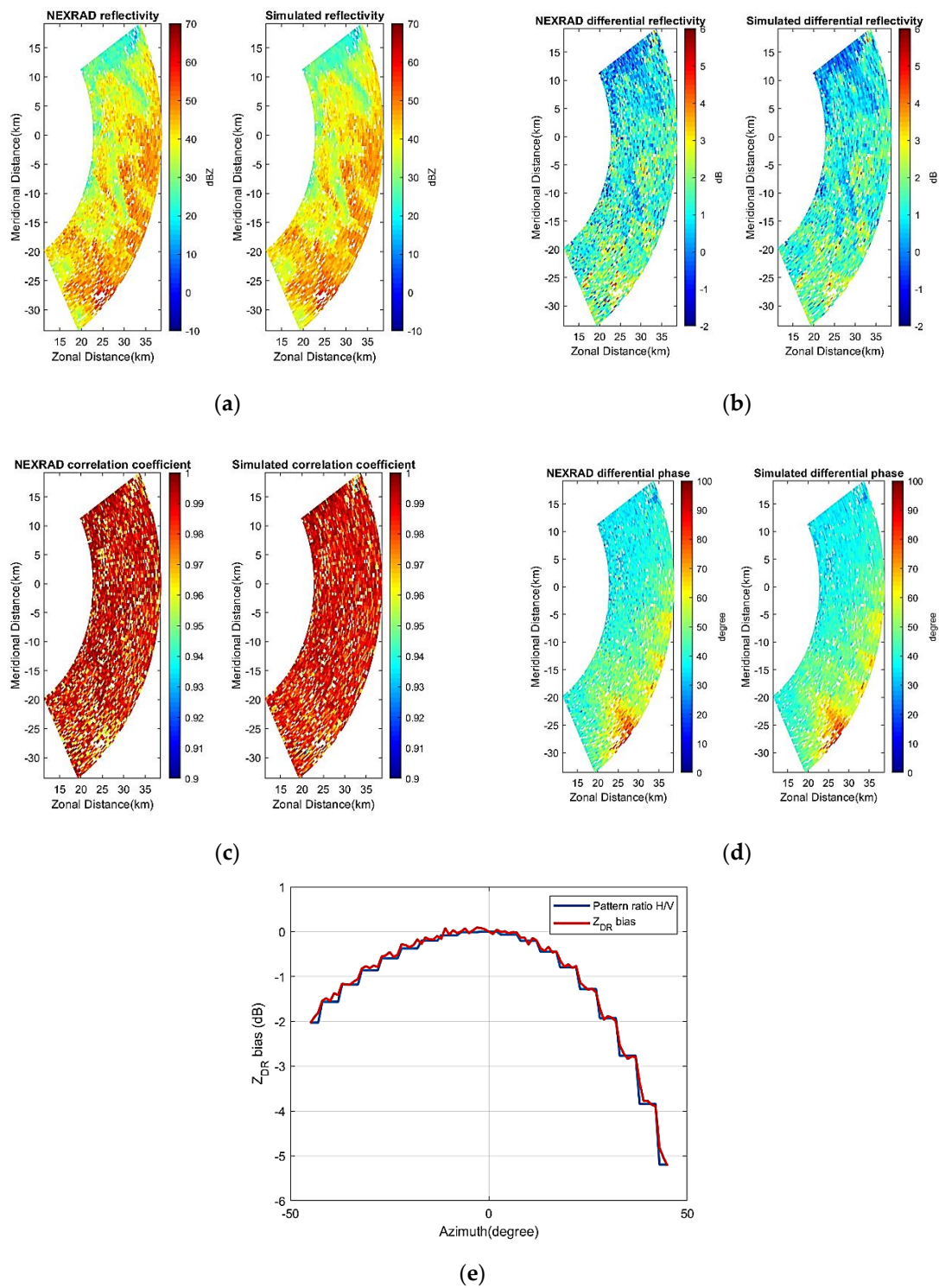
Figure 9. Simulated polarimetric radar moments generated from the advanced technology demonstrator (ATD) model of PASIM, and comparison with the "truth" weather fields for Case 2: (**a**) reflectivity, (**b**) differential reflectivity, (**c**) correlation coefficient, (**d**) differential phase, (**e**) averaged differential reflectivity bias along azimuth from −45° to 45°.

Table 5. System parameters of the simulated advanced technology demonstrator (ATD).

Radar Parameters	Values
Frequency	2800 MHz
Array size	4 × 4 m
Number of subarrays	100
Beamwidth	Azimuth 1.8°
First sidelobe	−30.3 dB
Waveform	Rectangular pulse
Pulse width	1.6 µs
Pulse repetition frequency	300 Hz
Range resolution	250 m
Peak power	768 W per subarray
Noise figure	2.7 dB

3.3.3. Cylindrical Polarimetric Phased-Array Radar (CPPAR) System

As the second specific system example, PASIM was configured to simulate S-band CPPAR systems with various diameters. There were two purposes for this simulation. Firstly, we wanted to justify the data quality of CPPAR based on commutative scanning. Secondly, we wanted to guide the selection of CPPAR diameters that can achieve acceptable data quality.

The following example shows the PPI scans from a simulated 2-m-diameter CPPAR demonstrator, which is populated by 96 columns of the generic dual-polarized patch elements and uses a 90° sector (24 columns) to form a commutated beam with a beamwidth of 5.2° and the first sidelobe of −30.1 dB. The technical specifications of the simulated CPPAR demonstrator are listed in Table 6. The simulation results of polarimetric moments and the average Z_{DR} bias along all azimuth angles for the convective precipitation case are shown in Figure 10. Error statistics for Case 1 and Case 2 are provided in Section 3.3.4, respectively.

Table 6. System parameters of the simulated cylindrical polarimetric phased-array radar (CPPAR).

Radar Parameters	Values for 2-m CPPAR	Values for 10-m CPPAR
Frequency	2800 MHz	2800 MHz
Array size	2 m diameter	10 m diameter
Number of excited columns	24	156
Beamwidth	Azimuth 5.2°	Azimuth 1.1°
First sidelobe	−30.1 dB	−30.5 dB
Waveform	Rectangular pulse	Rectangular pulse
Pulse width	1.6 µs	1.6 µs
Pulse repetition frequency	300 Hz	300 Hz
Range resolution	250 m	250 m
Peak power	80 W per column	80 W per column
Noise figure	2.7 dB	2.7 dB

From Figure 10, we can find that all the simulated radar moments were smeared obviously compared with NEXRAD truth fields, as a result of the much broader beamwidth of the 2-m-diameter CPPAR, whose data quality cannot meet the NEXRAD requirements. Moreover, the system Z_{DR} bias fluctuated a lot around the two-way power pattern ratio at different azimuth directions, which was mainly caused by a beam smoothing effect.
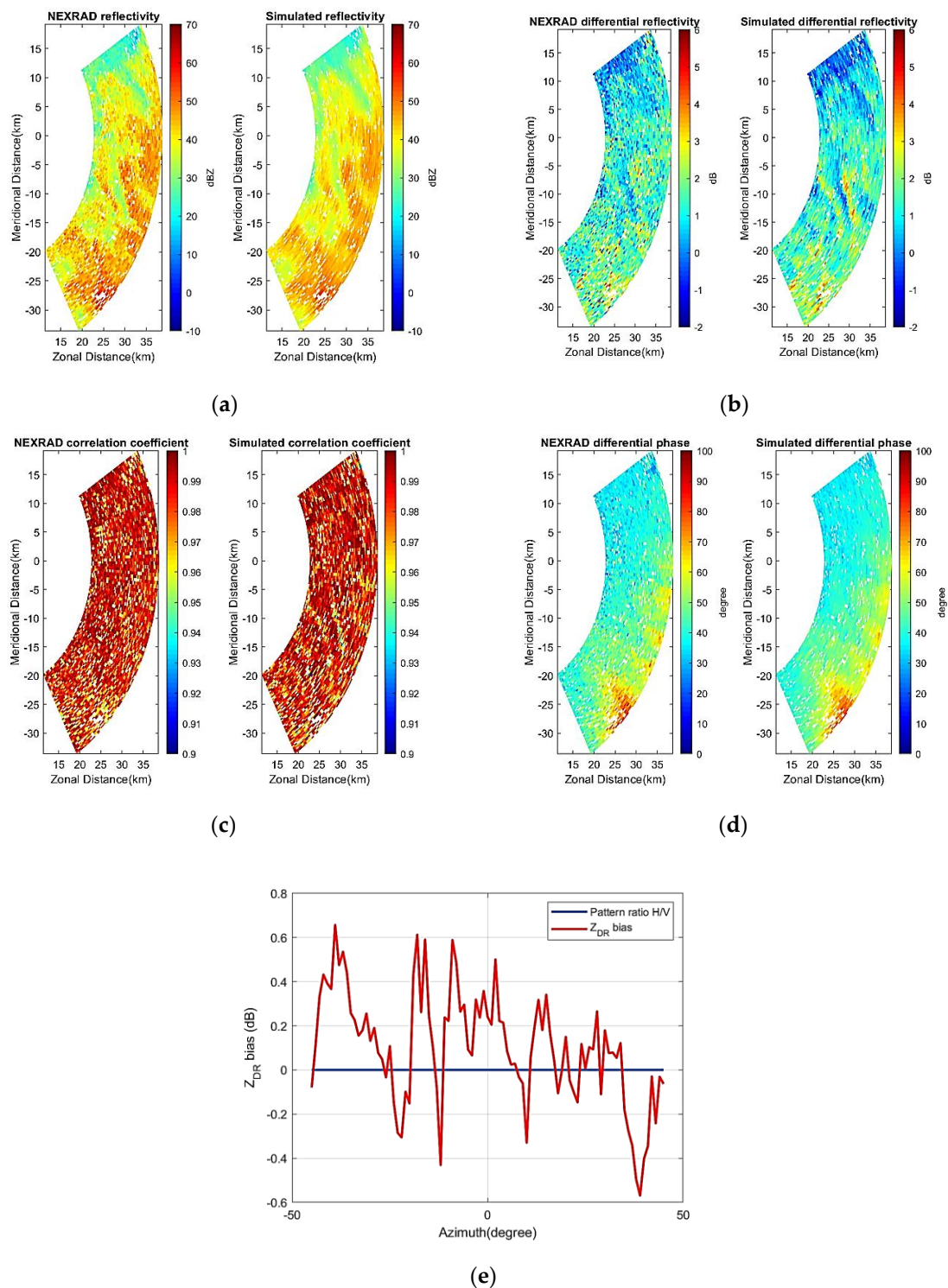
(**a**)   (**b**)

(**c**)   (**d**)

(**e**)

Figure 10. Simulated polarimetric radar moments generated from the 2-m-diameter cylindrical polarimetric phased-array radar (CPPAR) model of PASIM, and comparison with the "truth" weather fields for Case 2: (**a**) reflectivity, (**b**) differential reflectivity, (**c**) correlation coefficient, (**d**) differential phase, (**e**) averaged differential reflectivity bias along azimuth from −45° to 45°.

The other example shows the PPI scan data from a "full-size" (10-m-diameter) CPPAR, which is populated by 624 columns of the generic dual-polarized patch elements and uses a 90° sector (156 columns) to form a commutated beam with a beamwidth of 1.1° and the first sidelobe of −30.5 dB. The technical specifications of the simulated full-size CPPAR are listed in Table 6. The simulation

results of polarimetric moments and the average Z_{DR} bias along all azimuth angles for the convective precipitation case are shown in Figure 11. Error statistics for Case 1 and Case 2 are provided in Section 3.3.4, respectively.
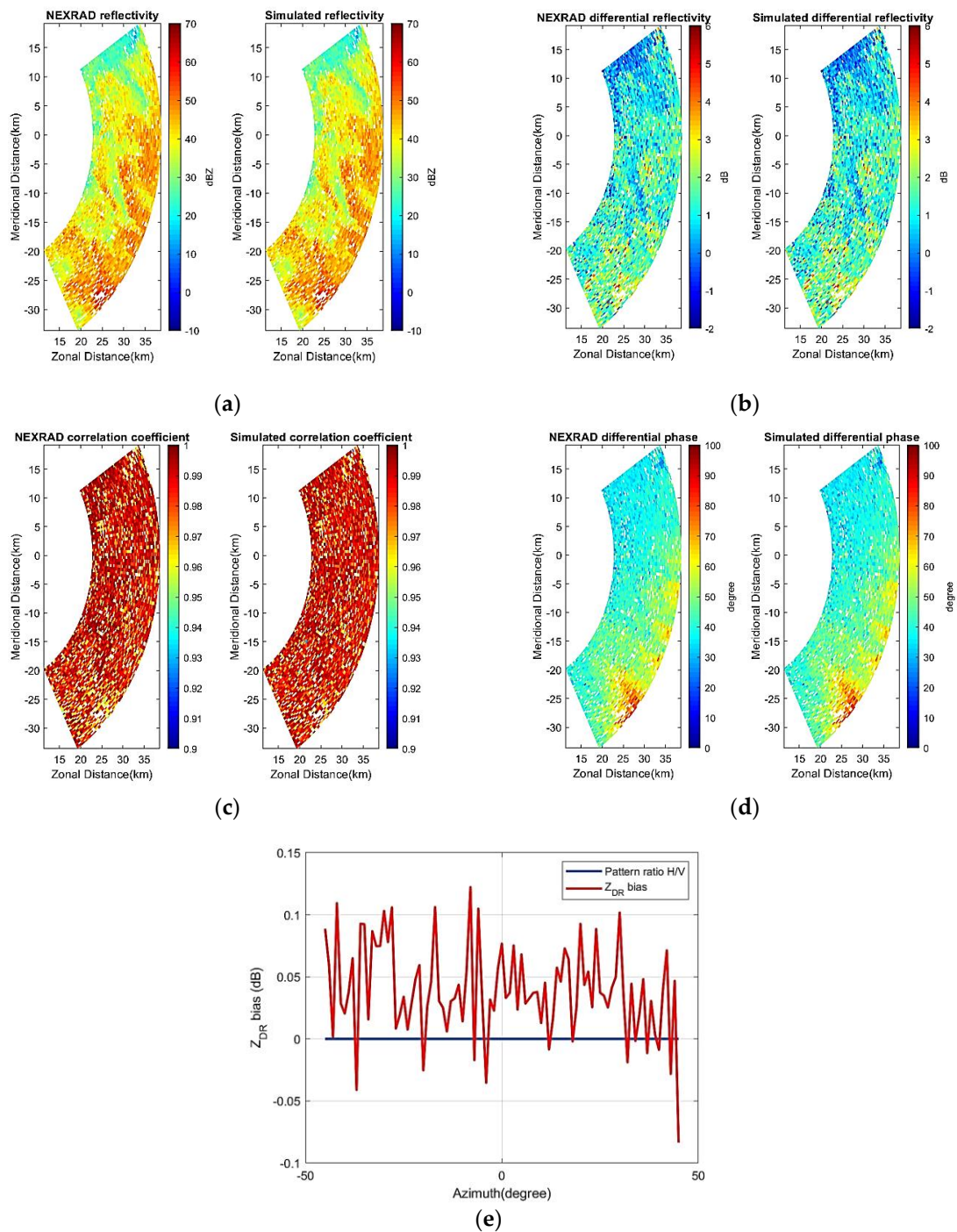

Figure 11. Simulated polarimetric radar moments generated from the 10-m-diameter CPPAR model of PASIM, and comparison with the "truth" weather fields for Case 2: (**a**) reflectivity, (**b**) differential reflectivity, (**c**) correlation coefficient, (**d**) differential phase, (**e**) averaged differential reflectivity bias along azimuth from −45° to 45°.

We can observe from Figure 11 that the 10-m-diameter CPPAR is likely to achieve the data quality that meets the NEXRAD requirements, and the system Z_{DR} bias was low for different azimuth

directions, which exhibits its advantage compared to the results from the ATD system example. The random fluctuation of Z_{DR} bias curve around the two-way power pattern ratio was mainly caused by sampling error and reflectivity gradient.

3.3.4. Discussion

Tables 7 and 8 summarize the PASIM basic data quality evaluation results for the three example systems. Here, standard deviation is used as an error statistic, as bias can be eliminated by the calibration process. We can see from the comparison of the results that, in terms of overall data quality, a full-size CPPAR is expected to obtain the results closest to the generic radar example. As comparisons, ATD and 2-m-diameter CPPAR cannot meet NEXRAD requirements, mainly due to their broader beamwidth. On the other hand, data quality results are also closely related to the weather scenarios; for example, a larger reflectivity gradient will lead to degraded data quality due to its contamination through sidelobes of antenna patterns.

Table 7. Summary of error statistics for the tornado scenario (Case 1).

Radar Variable	Generic Radar	ATD	2-m-diameter CPPAR	10-m-diameter CPPAR
Z_H	0.81 dB	1.66 dB	3.79 dB	0.82 dB
Z_{DR}	0.18 dB	0.39 dB	0.98 dB	0.21 dB
ρ_{hv}	0.008	0.01	0.016	0.008
ϕ_{DP}	1.19°	2.65°	5.66°	1.35°

Table 8. Summary of error statistics for the convective precipitation scenario (Case 2).

Radar Variable	Generic Radar	ATD	2-m-diameter CPPAR	10-m-diameter CPPAR
Z_H	0.78 dB	1.42 dB	2.84 dB	0.79 dB
Z_{DR}	0.17 dB	0.36 dB	0.87 dB	0.19 dB
ρ_{hv}	0.006	0.007	0.014	0.006
ϕ_{DP}	1.12°	2.41°	4.58°	1.22°

These data quality evaluation results may provide useful guidance for PAR designs. For example, antenna elements should be designed with special care to reduce sidelobes of the array pattern, which is especially important to ensure acceptable data quality in strong convective weather with a large reflectivity gradient. Low cross-polarization levels, matched co-polarization beam patterns, and stable phase difference for horizontal and vertical polarizations are required for accurate measurements of polarimetric moments. NLFM waveform may be an option for SENSR-type radar systems, which can achieve both low range sidelobes and good power efficiency, while special attention should be paid to the increased phase noise levels if a direct digital waveform synthesizer is used.

Currently, there are still some limitations of the PASIM simulations. Firstly, for simplicity, uniform drop size was assumed in weather target modeling. However, to characterize the microphysical properties of precipitation, a more realistic drop size distribution model such as Gamma distribution may be used. Secondly, for the radar transceiver nonlinearity model, only the simple Saleh model was used in the current simulation, while a more accurate model for solid-state transceivers will be incorporated in the future, based on specific hardware designs and their laboratory characterizations.

4. Conclusions and Future Work

In this paper, an end-to-end PAR system simulator called PASIM, which was developed for predicting the data quality of future weather radars, was described. Based on the novel concept of time-domain, electronics-incorporated models, we demonstrated the example usages of PASIM, such as the impact of various pulse compression waveforms, the effect of the instability of channel electronics, nonlinear distortion, random amplitude and phase errors in array channels, and the quantization error of array phase shifters. Weather radar moment data qualities for multiple specific radar designs were

evaluated, including a generic radar, a planar array radar, and cylindrical array radars with various sizes in the context of two different weather scenarios.

PASIM simulation results further confirm the following:

(1) Antenna elements should have low sidelobes and cross-polarization levels, matched co-polarization beam patterns, and stable phase difference between horizontal and vertical polarizations to achieve accurate measurements of polarimetric radar moments.

(2) The NLFM waveform may be an option to meet the MPAR requirements, which can achieve both low range sidelobe levels favorable to convective weather observation, and good power efficiency favorable to weak echo observation.

(3) As an example of channel electronic instability, HPA nonlinearity will distort waveform, resulting in increased range sidelobes. Random amplitude and phase errors in array channels, and the quantization error of phase shifters will distort the antenna pattern by raising sidelobes and reducing gain. All of these will cause measurement errors in weather scenarios having a large reflectivity gradient.

(4) Array manifolds and sizes have large impacts on polarimetric radar measurement. A planar array will induce differential reflectivity bias as its beam steers away from its broadside, while a 10-m-diameter cylindrical array is likely to achieve data quality comparable to NEXRAD.

Better modeling of array channel-to-channel couplings will be developed for the next step. Improved RF transceiver models will be studied. Moreover, to model the interactions between pulse compression waveforms and distributed weather scatterers in the time domain, impulse response (IR) will be added in PASIM to improve the transient system simulations. Such innovation may reveal certain characteristics in the scattered electric field from weather resolution volumes, which may have an impact on the return signals [29–31]. For weather target modeling, a more realistic drop size distribution model will be included in the next step to characterize the microphysical properties of precipitation. Further validation of PASIM using measured weather data by actual phased-array radar testbeds, once they are available, is anticipated.

Author Contributions: Z.L.: Designed and implemented the PASIM software, obtained system data quality evaluation results, and prepared most of the manuscript. S.P.: Established the original idea and initial studies of the system simulation with phased array electronics modeling. Y.Z.: Established the original concepts of PASIM and architecture-specific system modeling. G.Z.: Provided important guidance of the fundamental models and algorithms for weather radar signal processing. R.D.: Provided funding support and collaboration from US government research team, NEXRAD radar information, and guidance of the simulation verifications.

Conflicts of Interest: The authors declare no conflicts of interest.

References

1.　Weber, M.E.; Cho, J.Y.N.; Thomas, H.G. Command and control for multifunction phased array radar. *IEEE Trans. Geosci. Remote Sens.* **2017**, *55*, 5899–5912. [CrossRef]

2.　Zrnić, D.S. Simulation of weatherlike Doppler spectra and signals. *J. Appl. Meteorol.* **1975**, *14*, 619–620. [CrossRef]

3.　Galati, G.; Pavan, G. Computer simulation of weather radar signals. *Simul. Pract. Theory* **1995**, *3*, 17–44. [CrossRef]

4.　Torres, S.M. Estimation of Doppler and Polarimetric Variables for Weather Radars. Ph.D. Thesis, University of Oklahoma, Norman, OK, USA, 2001.

5.　Cheong, B.L.; Palmer, R.D.; Xue, M. A time series weather radar simulator based on high-resolution atmospheric models. *J. Atmos. Ocean. Technol.* **2008**, *25*, 230–243. [CrossRef]

6. Li, Z.; Zhang, Y.; Zhang, G.; Brewster, K. A microphysics-based simulator for advanced airborne weather radar development. *IEEE Trans. Geosci. Remote Sens.* **2011**, *49*, 1356–1373. [CrossRef]

7. Byrd, A.D.; Ivić, I.R.; Palmer, R.D.; Isom, B.M.; Cheong, B.L.; Schenkman, A.D.; Xue, M. A weather radar simulator for the evaluation of polarimetric phased array performance. *IEEE Trans. Geosci. Remote Sens.* **2016**, *54*, 4178–4189. [CrossRef]

8. Barcaroli, E.; Lupidi, A.; Facheris, L.; Cuccoli, F.; Chen, H.; Chandrasekar, V. A validation procedure for a polarimetric weather radar signal simulator. *IEEE Trans. Geosci. Remote Sens.* **2019**, *57*, 609–622. [CrossRef]

9. Schvartzman, D.; Curtis, C.D. Signal processing and radar characteristics (SPARC) simulator: A flexible dual-polarization weather-radar signal simulation framework based on preexisting radar-variable data. *IEEE J. Sel. Top. Appl. Earth Observ.* **2019**, *12*, 135–150. [CrossRef]

10. Wang, S. Waveform and Transceiver Optimization for Multi-Functional Airborne Radar through Adaptive Processing. Ph.D. Thesis, University of Oklahoma, Norman, OK, USA, 2013.

11. Tua, C.G.; Pratt, T.; Zaghloul, A.I. A study of interpulse instability in gallium nitride power amplifiers in multifunction radars. *IEEE Trans. Microw. Theory Tech.* **2016**, *64*, 3732–3747. [CrossRef]

12. Chen, H.; Gentile, R. Phased array system simulation. In Proceedings of the 2016 IEEE International Symposium on Phased Array Systems and Technology (PAST), Waltham, MA, USA, 18–21 October 2016.

13. Nepal, R.; Zhang, Y.; Blake, W. Sense and avoid airborne radar implementations on a low-cost weather radar platform. *Aerospace* **2017**, *4*, 11. [CrossRef]

14. Helmus, J.; Collis, S. The Python ARM Radar Toolkit (Py-ART), a library for working with weather radar data in the Python programming language. *J. Open Res. Softw.* **2016**, *4*, e25. [CrossRef]

15. Heistermann, M.; Collis, S.; Dixon, M.J.; Giangrande, S.; Helmus, J.J.; Kelley, B.; Koistinen, J.; Michelson, D.B.; Peura, P.; Pfaff, T.; et al. The emergence of open-source software for the weather radar community. *Bull. Am. Meteorol. Soc.* **2015**, *96*, 117–128. [CrossRef]

16. Meikle, H. *Modern Radar System*, 2nd ed.; Artech House Publishers: Norwood, MA, USA, 2008; pp. 51–79.

17. Saleh, A.A.M. Frequency-independent and frequency-dependent nonlinear models of TWT amplifiers. *IEEE Trans. Commun.* **1981**, *29*, 1715–1720. [CrossRef]

18. Ge, Z.; Huang, P.; Lu, W. Matched NLFM pulse compression method with ultra-low sidelobes. In Proceedings of the 2008 European Radar Conference, Amsterdam, The Netherlands, 30–31 October 2008.

19. Zhang, G. *Weather Radar Polarimetry*; CRC Press: Boca Raton, FL, USA, 2016; p. 304.

20. Doviak, R.J.; Zrnić, D.S. *Doppler Radar and Weather Observations*, 2nd ed.; Dover Publications, Inc.: Mineola, NY, USA, 2006; p. 562.

21. Bringi, V.N.; Chandrasekar, V. *Polarimetric Doppler Weather Radar: Principles and Applications*; Cambridge University Press: Cambridge, UK, 2001; p. 636.

22. NOAA/NSSL Report. Available online: https://www.nssl.noaa.gov/publications/wsr88d_reports/SHV_statistics.pdf (accessed on 8 January 2017).

23. Stailey, J.E.; Hondl, K.D. Multifunction phased array radar for aircraft and weather surveillance. *Proc. IEEE* **2016**, *104*, 649–659. [CrossRef]

24. Ivić, I.R. Options for polarimetric variable measurements on the MPAR Advanced Technology Demonstrator. In Proceedings of the 2018 IEEE Radar Conference, Oklahoma City, OK, USA, 23–27 April 2018.

25. Zhang, G.; Doviak, R.J.; Zrnić, D.S.; Palmer, R.D.; Lei, L.; Al-Rashid, Y. Polarimetric phased-array radar for weather measurement: A planar or cylindrical configuration? *J. Atmos. Ocean. Technol.* **2011**, *28*, 63–72. [CrossRef]

26. Fulton, C.; Salazar, J.L.; Zhang, Y.; Zhang, G.; Kelly, R.; Meier, J.; McCord, M.; Schmidt, D.; Byrd, A.D.; Bhowmik, L.M.; et al. Cylindrical polarimetric phased array radar: Beamforming and calibration for weather applications. *IEEE Trans. Geosci. Remote Sens.* **2017**, *55*, 2827–2841. [CrossRef]

27. Lei, L. Theoretical Analysis and Bias Correction for Planar and Cylindrical Polarimetric Phased Array Weather Radar. Ph.D. Thesis, University of Oklahoma, Norman, OK, USA, 2014.

28. Lei, L.; Zhang, G.; Doviak, R.J.; Karimkashi, S. Comparison of theoretical biases in estimating polarimetric properties of precipitation with weather radar using parabolic reflector, or planar and cylindrical arrays. *IEEE Trans. Geosci. Remote Sens.* **2015**, *53*, 4313–4327. [CrossRef]

29. Perera, S.; Zhang, Y.; Zrnić, D.S.; Doviak, R.J. Scalable EM simulation and validations of dual-polarized phased array antennas for MPAR. In Proceedings of the 2016 IEEE International Symposium on Phased Array Systems and Technology (PAST), Waltham, MA, USA, 18–21 October 2016.

30. Perera, S.; Zhang, Y.; Zrnić, D.S.; Doviak, R.J. Electromagnetic simulation and alignment of dual-polarized array antennas in multi-mission phased array radars. *Aerospace* **2017**, *4*, 7. [CrossRef]
31. Perera, S. Physical Knowledge Based Scalable Phased Array Antenna Modeling for Radar Systems. Ph.D. Thesis, University of Oklahoma, Norman, OK, USA, 2016.